Supplementary Information

Deep Levels, Charge Transport and Mixed Conductivity in Organometallic Halide Perovskites

Artem Musiienko[1*], Pavel Moravec[1], Roman Grill[1], Petr Praus[1], Igor Vasylchenko[1], Jakub Pekarek[1], Jeremy Tisdale[2], Katarina Ridzonova[1], Eduard Belas[1], Lucie Abelová[3,4], Bin Hu[2], Eric Lukosi[5], Mahshid Ahmadi[2*]

[1]*Institute of Physics, Charles University, Prague, 121 16, Czech Republic*
[2]*Joint Institute for Advanced Materials, Department of Materials Science and Engineering, University of Tennessee, Knoxville, TN 37996, USA*
[3] *Institute of Physics, Academy of Sciences of the Czech Republic, Prague, Czech Republic.*
[4] *Electrical Engineering, Czech Technical University in Prague, Prague, Czech Republic*
[5]*Joint Institute for Advanced Materials, Department of Nuclear Engineering, University of Tennessee, Knoxville, TN 37996, USA*

*Corresponding authors email:
M. Ahmadi: mahmadi3@utk.edu, A. Musiienko: musienko.art@gmail.com

Methods

Single crystal growth

Lead bromide (≥98%) and methylammonium bromide (MABr) were purchased from Alfa Aesar, Dimethylformamide (DMF) (anhydrous, 99.8%) were purchased from Sigma Aldrich. All precursors and solvents were used as received. In the first method, single crystals of $MAPbBr_3$ were grown via an inverse temperature crystallization (ITC) method[92] with a slightly modified temperature gradient (Samples No. 1 and No. 2). In this method, MABr and $PbBr_2$ were mixed with 1:0.8 molar ratio in 1 mL DMF solvent. The solution was stirred for 1 h and then filtered using a 0.2 μm PTFE filter. The solution was then placed in an oil bath on a hot plate and $MAPbBr_3$ single crystals were grown by slow temperature increase during overnight to 75 °C. After growth, the crystals were

washed using dichloromethane (DCM). Samples typical resistivity of 3×10^8 Ωcm was found from four-point resistivity measurements.

In the second method (sample No. 3), $MAPbBr_3$ single crystals were grown by dissolving $PbBr_2$ and MABr in 2.5 ml DMF at 55 ° C for 1-1.5 hr. Then, 75 µl of HCOOH was added to the solution, and after the dissolution of the formed precipitate, the solution was filtered through a syringe filter with a pore size of 0.2 µm. The solution was heated to 70 ° C for 15 minutes and then to 73 ° C for 40 minutes. During this time, many small crystals formed in solution as seed crystals. Next, the seed crystals were placed in a fresh preheated solution, where they could grow larger at 55 ° C for 19 h. This cycle was repeated 2 more times for growing larger crystals. The grown crystals were then dried with Kimwipe. The whole crystallization was performed in the glovebox. Samples typical resistivity of 5×10^7 Ωcm was found from four-point resistivity measurements.

UV-Visible and Photoluminescence spectroscopy

UV-visible and Photoluminescence spectroscopy was performed to confirm $MAPbBr_3$ band gap energy (**Figure S1**). From UV-Visible absorption spectrum a sharp edge is observed at 540 nm with the extrapolated bandgap energy of around 2.2 eV, in agreement with literature[92]. The primary photoluminescence emission peak is centered at 530 nm, and a secondary peak is centered at 575 nm due to strong self-absorption, which are consistent with published results[93].

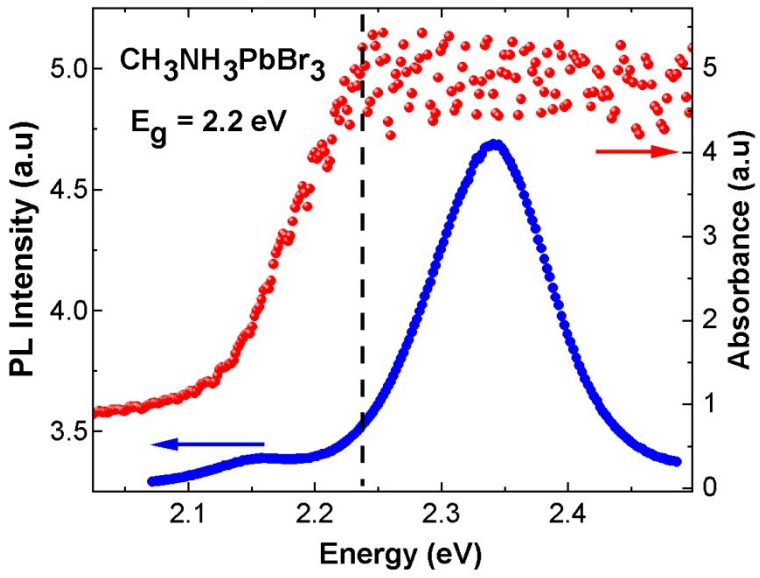

Figure S1. UV-Visible absorption (red circles) and PL spectra (blue circles) of $MAPbBr_3$ single crystals.

Sample preparation for Photo Hall effect spectroscopy measurements

Prior to contacts deposition, $MAPbBr_3$ samples were initially rinsed in pure toluene and then dried using compressed dry air. The $MAPbBr_3$ single crystals were prepared in two different ways. The first sample was glued on a silicone support with a commercially available acrylate lacquer (30 wt. % in toluene). The front crystal face was mechanically covered by a mask made of aluminum foil. The second sample was masked using only acrylate lacquer. The latter was dried by keeping crystals in the open air for 10 minutes. Afterward, gold contacts were evaporated in 10^{-5} mbar vacuum; the resulting samples were taken off the supports in pure toluene, additionally rinsed in the same solution and dried in air flow. To prevent material degradation between measurements single crystals were kept in dark condition in a sealed container over both moisture and oxygen absorbents.

Photo Hall effect spectroscopy setup

The principle of classical Hall-effect measurements and photo-Hall effect spectroscopy are depicted in Figure S2. Bar-like samples were used in the classical six-contact Hall-bar shape convenient for galvanomagnetic measurements. Samples with typical dimensions of $1\times2.5\times9$ mm^3 were used for galvanomagnetic measurements. Hall-bar shape approximates the ideal geometry for for measuring the Hall effect, in which the constant current density flows along the long axis of a rectangular solid, perpendicular to an applied external magnetic field $\boldsymbol{B}$. The ideal six-contact Hall-bar geometry is symmetrical. Side contact pairs are placed symmetrically about the midpoint of the sample's long axis and located oppositely to each other. This geometry allows us two equivalent sets of measurements of resistivity and Hall effect to eliminate possible sample non-homogeneity. Hall voltage contacts must be located far enough from the sample's ends to avoid short circuit in the Hall voltage that could lead to an underestimated actual Hall coefficient. The longitudinal voltage V, current I, and the transverse Hall voltage V_H were measured directly from the experiment. To calculate the resistivity and Hall mobility we used the average values including different orientations of the applied current and magnetic field. Measurements were performed at room temperature with a constant magnetic field B of 1 T.

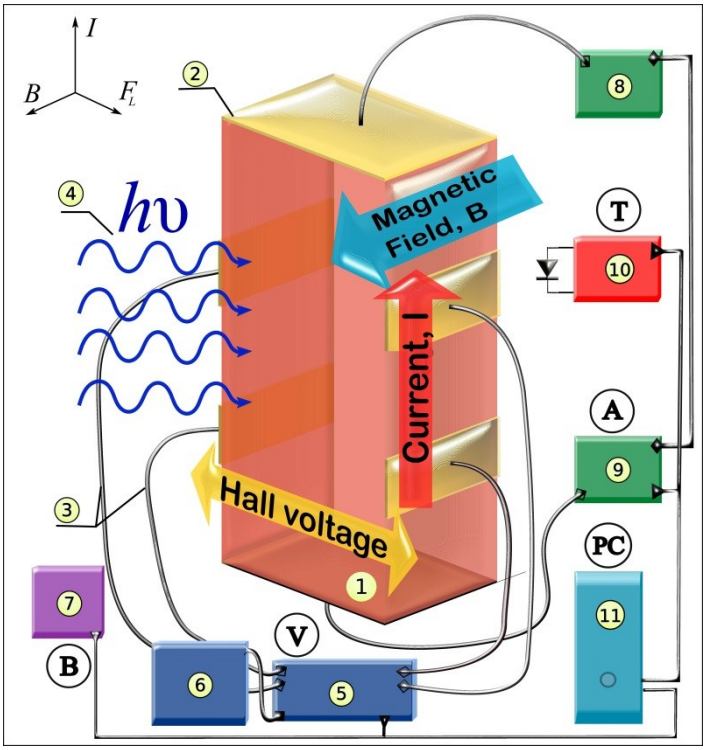

Figure S2 Experimental set-up for conventional Hall effect, photo-Hall and photoconductivity measurements: 1 sample, 2 gold contacts, 3 silver wires, 4 monochromatic light, 5 switch system with Hall effect card (Keithley 7001), 6 system multimeter (Keithley 2000), 7 source for the electromagnet (15 A), 8 current source (Keithley 220), 9 picoammeter (Keithley 485), 10 GaAlAs diode for the temperature detection, 11 PC.

$MAPbBr_3$ samples were studied by PHES in the energy range of 0.6-2.4 eV. The PhC spectra are shown in **Figure S3** in a linear scale. As can be seen, the initial photon energies started from 0.6 eV when the first increase was detected at 1.05 eV. The second threshold is detected at 1.48 eV.

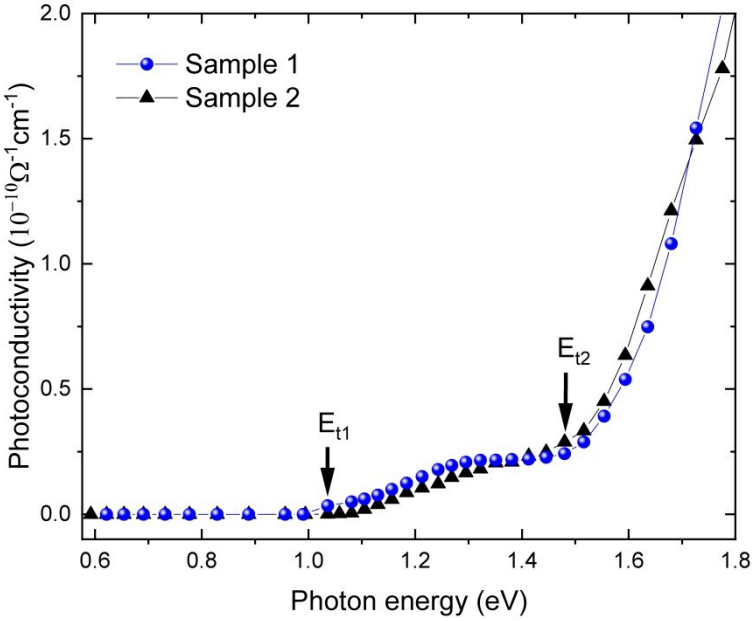

Figure S3 Photoconductivity spectra of two single crystals of $MAPbBr_3$ as a function of photon energy. Vertical arrows show the deep level threshold energy. Spectra are plotted in linear scale to show low photon energy data where no photoconductivity response was detected.

Hall effect in material with mixed electronic and ionic conductivity:

The increase of Hall coefficient and Hall signal enhancement can be explained by ions contribution as was qualitatively explained in Eq. (7) and Eq. (8). Here we have derived the ion contribution in detail:

The Hall signal in a semiconductor material without mixed conductivity follows below equation:

$$R_{H1} = \frac{V_{H1} d}{IB} = \frac{1}{q_e p} \quad \textbf{(14)}$$

The Hall voltage V_{HI} is defined by the hole concentration p. If now we consider a semiconductor with mixed conductivity, Eq. (14) is modified to:

$$R_{H2} = \frac{V_{H2}d}{I \cdot B} = \frac{1}{q_e p\left(1 + \frac{\mu_i N_i}{\mu_p p}\right)^2} \quad \textbf{(15)}$$

As can be seen, the Hall signal is suppressed by the ionic impact $\mu_i N_i$:

$$\frac{1}{q_e p} > \frac{1}{q_e p\left(1 + \frac{\mu_i N_i}{\mu_p p}\right)^2} \quad \textbf{(16)}$$

The Hall signal in a semiconductor with pure electronic conductivity is higher ($V_{H1} > V_{H2}$) however, the Hall signal can be enhanced by the light illumination by increasing hole concentration as it was shown in the manuscript.

Here, R_{H1} and R_{H2} were plotted as a function of hole concentration in **Figure S4**. The value of $\mu_i N_i$ product is fixed to 10^{11} $cm^{-1}V^{-1}s^{-1}$ for simplicity. As it can be seen, the generation of free holes leads to an increase in Hall coefficient while ion free Hall coefficient decreases.

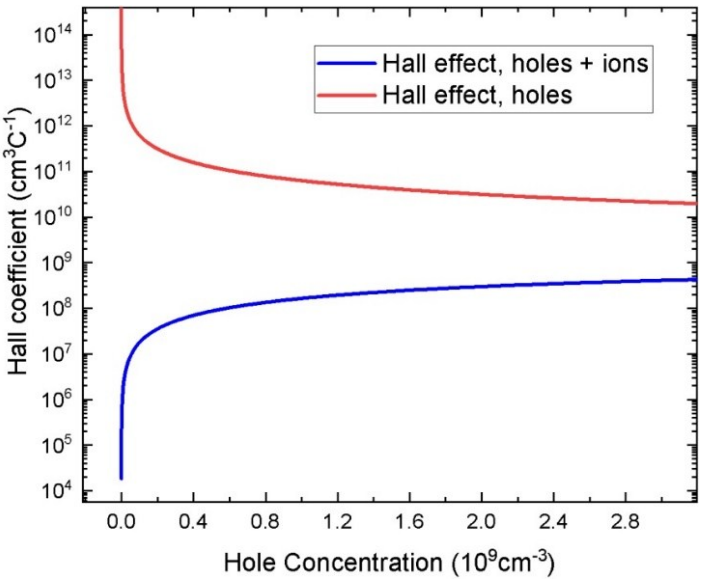

Figure S4: Plot of Hall coefficient as a function of holes concentration.

Consequently during photoexcitation when the hole concentration dominant the ion concentration, the Hall mobility is increased by free hole generation as seen in **Figure S4**. Note that Hall mobility does not directly represent drift mobility as derived in Eq. (4). To explicitly show this we have plotted μ_H as a function of hole concentration (according to Eq. (4)).

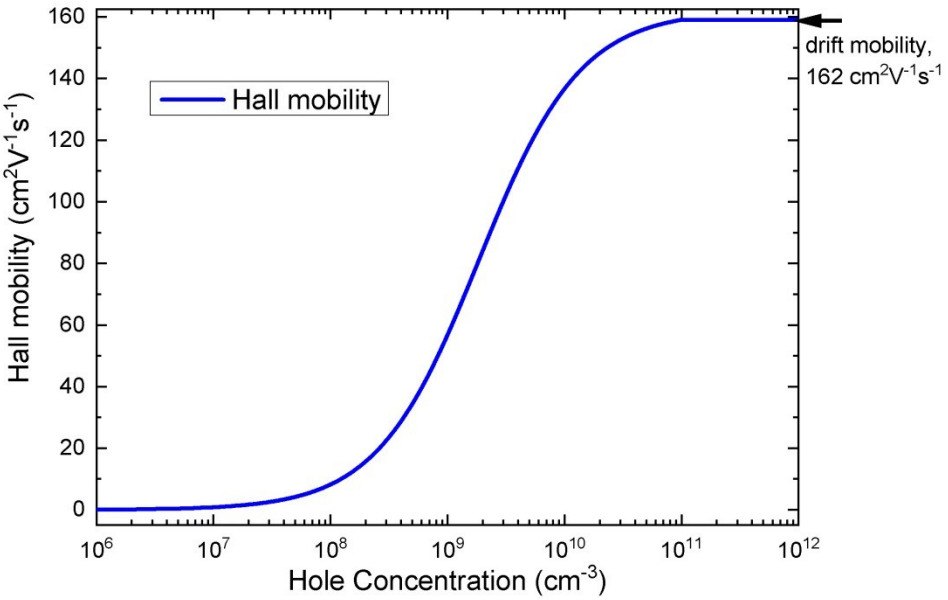

Figure S5: Hall mobility as a function of hole concentration in semiconductor with mixed conductivity type.

As can be seen in **Figure S5**, Hall mobility starts from very low values <1 $cm^2V^{-1}s^{-1}$ and then converges to hole drift mobility at higher hole concentration. Note that it is well established that ion concentration *Ni* can also enhance under illumination in OMHPs[66], but as it was shown in the manuscript this change is two orders of magnitude lower than the impact of free holes in the photoconductivity. Therefore, a slight increase in the ion concentration does not influence PHES deep level detection.

Photo-Hall in $MAPbBr_3$ single crystals grown with the second method:

Deep levels with activation energies E_V + 1.05 eV, E_V + 1.5 eV, and E_V + 1.9 eV (E_C - 1.9 eV) were detected by PHES in $MAPbBr_3$ as shown in **Figure S6.** This sample was grown with a slightly different method in the lab of Czech Technical University in Prague (Details can be found in materials section).

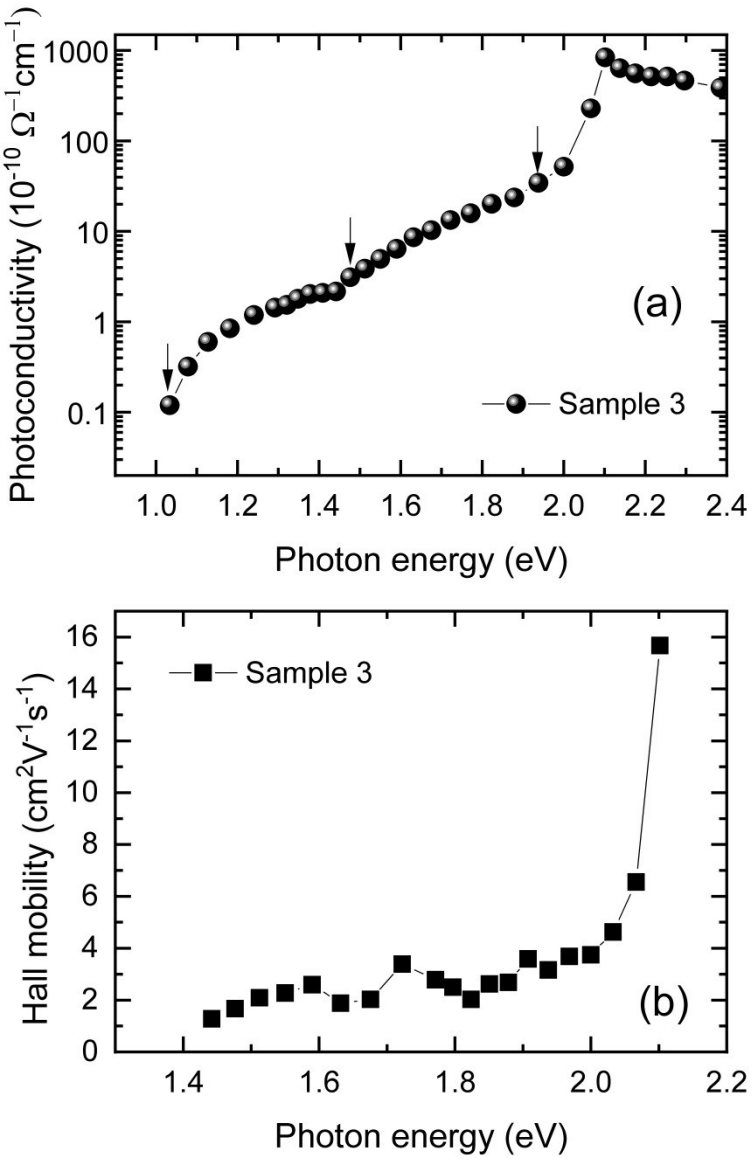

143

144 **Figure S6:** (a) Photoconductivity and (b) Hall mobility spectra of $MAPbBr_3$ single crystals grown in
145 another laboratory as a function of photon energy. Vertical arrows show the deep level threshold
146 energy.

147 **Single crystal degradation test**

148 Indeed, it is well established that the optoelectrical properties of OMHP can be highly influenced by
149 the environmental atmosphere[5,94,95]. In addition, degradation of OMHPs can be further enhanced
150 under photoexcitation and external electric field. While single crystals of $MAPbBr_3$ maintain an
151 impressive stability and the original orange color after exposure in ambient air for several months. In
152 any study performed under ambient condition, it is almost impossible to prevent surface degradation
153 or contamination. However, we expect that the possible degradation occurs only on the top few nm
154 surface of the single crystals during the time frame of these measurements[76]. In principle, water

intercalating to the bulk of single crystals could change the device conductivity/resistivity as was shown in previous studies[96–98]. In this study, single crystal resistivity was measured by four probe resistivity and the single crystals showed an average resistivity of $(1.90 \pm 0.04) \times 10^8$ Ωcm before and $(1.96 \pm 0.03) \times 10^8$ Ωcm after PHES. The negligible changes in resistivity before and after the measurements suggest that within the time frame of our measurements, in terms of apparent resistivity the water has not infiltrated in the bulk of single crystals upon exposure to the ambient condition and hasn't influenced on the resulting DLs.

Time of flight measurements

$MAPbBr_3$ single crystals with a typical thickness of 1.8 mm are studied by laser-induced transient current measurements. For this experiment, two opposite gold contacts were deposited on single crystal $MAPbBr_3$ by thermal evaporation. A DC bias, varying between 6 V and 12 V, was applied to the sample. Anode side of the sample was illuminated by the above-bandgap pulse laser, that was powered by the amplified output of the arbitrary waveform generator. Both hole and electron signals were separately collected. Incident probe pulses had the wavelength of 450 nm, pulse width of 100 ns, and the repetition rate was set to 100 Hz. We applied neutral density optical filter to attenuate the light pulse peak power to ~ 5 mW. So that, the used probe pulse intensity is weak enough not to affect the properties of the studied material. We use an in-house designed wide bandwidth high frequency voltage amplifier to record CWF by the digital sampling oscilloscope (4 GHz, 11 bit resolution). The detailed scheme of the ToF apparatus was shown in our previous works[25,99].

Shockley-Read-Hall recombination theory

The Shockley-Read-Hall hole recombination-generation rate[100] complemented by illumination-mediated deep level - band transitions is given by relations

$$\frac{\partial p}{\partial t} = -\sum_i U_i^h + \sum_i I_{vi}, \tag{17}$$

$$U_i^h = \sigma_{hi} \nu_h \left[n_{ti} p - (N_{ti} - n_{ti}) p_{1i} \right], \tag{18}$$

$$I_{vi} = I \tilde{\alpha}_{hi} (N_{ti} - n_{ti}). \tag{19}$$

where n, p, $n_{ti}(p_{ti},)$, U_i^h, are the densities of free electrons, free holes, electrons(holes) trapped in the i-th level, and hole net recombination rate at the i-th level. The quantities defining recombination rates n_{ti}, N_{ti}, σ_{hi}, and ν_h in Eqs. (17-18) are intrinsic carrier density, i-th DL density, hole thermal capture cross section, and hole thermal velocity. Symbol p_{1i} stands for electron and hole densities in

case of Fermi level E_F being set equal to the DL ionization energy E_{ti}[100]. The effect of illumination on the i-th DL occupancy is defined by I_{ci} (I_{vi}) generation rate from i-th level to the conduction (valence) band where I, $\tilde{\alpha}_{ei}$, and $\tilde{\alpha}_{hi}$ are the photon flux and photon capture cross sections relevant to the conduction and valence band transition respectively. The simplified version of Eq. (17) in the case of single DL is used to find the hole capture cross section in this paper. The hole lifetimes τ can be found by relation

$$\tau = \frac{1}{\sum_i v_h \sigma_{hi} n_{ti}} \tag{20}$$

The inter-band light-induced generation rate and bimolecular recombination rate are neglected in the case of sub-bandgap illumination.